LIMNOLOGY and OCEANOGRAPHY

ASLO

Limnol. Oceanogr. 60, 2015, 2059–2078

doi: 10.1002/lno.10155

Rapid growth and concerted sexual transitions by a bloom of the harmful dinoflagellate *Alexandrium fundyense* (Dinophyceae)

Michael L. Brosnahan,*[1] Lourdes Velo-Suárez,[2] David K. Ralston,[3] Sophia E. Fox,[4] Taylor R. Sehein,[1] Alexi Shalapyonok,[1] Heidi M. Sosik,[1] Robert J. Olson,[1] Donald M. Anderson[1]

[1]Biology Department, Woods Hole Oceanographic Institution, Woods Hole, Massachusetts
[2]Department Dynamiques de l'Environment Côtier, Institut Français de Recherche pour L'Exploitation de la MER, Plouzané, France
[3]Applied Ocean Physics and Engineering Department, Woods Hole Oceanographic Institution, Woods Hole, Massachusetts
[4]Cape Cod National Seashore, National Park Service, Wellfleet, Massachusetts

Abstract

Transitions between life cycle stages by the harmful dinoflagellate *Alexandrium fundyense* are critical for the initiation and termination of its blooms. To quantify these transitions in a single population, an Imaging FlowCytobot (IFCB), was deployed in Salt Pond (Eastham, Massachusetts), a small, tidally flushed kettle pond that hosts near annual, localized *A. fundyense* blooms. Machine-based image classifiers differentiating *A. fundyense* life cycle stages were developed and results were compared to manually corrected IFCB samples, manual microscopy-based estimates of *A. fundyense* abundance, previously published data describing prevalence of the parasite *Amoebophrya*, and a continuous culture of *A. fundyense* infected with *Amoebophrya*. In Salt Pond, a development phase of sustained vegetative division lasted approximately 3 weeks and was followed by a rapid and near complete conversion to small, gamete cells. The gametic period (~3 d) coincided with a spike in the frequency of fusing gametes (up to 5% of *A. fundyense* images) and was followed by a zygotic phase (~4 d) during which cell sizes returned to their normal range but cell division and diel vertical migration ceased. Cell division during bloom development was strongly phased, enabling estimation of daily rates of division, which were more than twice those predicted from batch cultures grown at similar temperatures in replete medium. Data from the Salt Pond deployment provide the first continuous record of an *A. fundyense* population through its complete bloom cycle and demonstrate growth and sexual induction rates much higher than are typically observed in culture.

Blooms of toxic dinoflagellates within the genus *Alexandrium* are among the most widespread and dangerous harmful algal blooms (HABs) globally, and cause significant ecological, economic and public health impacts to temperate and subarctic coastal areas worldwide (Anderson et al. 2012). Toxic species within the genus produce saxitoxins, a class of neurotoxins that selectively block sodium ion channels in animals. Consumption of animals contaminated with toxic *Alexandrium* causes paralytic shellfish poisoning (PSP), a syndrome that can lead to respiratory arrest and death in humans. Therefore, understanding the physiological and ecological factors that control the timing and biogeography of *Alexandrium* blooms is important for ensuring seafood safety.

For many *Alexandrium* species the recurrence and spread of blooms depends on the formation of benthic resting cysts, a diploid life cycle stage that is highly resistant to temperature, salinity, and mechanical stress (Pfiester and Anderson 1987). The cysts themselves can remain dormant and viable for decades, leaving contaminated areas at risk for PSP even if conditions are rarely favorable for new blooms (Miyazono et al. 2012). Cyst formation occurs during the maturation of zygote cells and is therefore deeply entwined with the sexual life cycle of these organisms. The factors controlling when and to what extent *Alexandrium* undergo sex are not well understood but are important determinants of bloom intensity and onset of termination (Li et al. 2009; Anderson et al. 2013). Moreover, seasonal temperature patterns and other climate-related factors that determine bloom initiation and development are also likely to affect sexual

*Correspondence: mbrosnahan@whoi.edu

induction and new cyst production, altering the range and impact of PSP events under future climate conditions (Hallegraeff 2010).

Two longstanding obstacles to documenting sexual events in *Alexandrium* blooms have been the difficulty of differentiating their vegetative, gamete and planozygote stages and also the necessity of following single populations through time. A previous study advanced an approach that addresses both challenges through a combination of imaging flow cytometry, quantitative DNA content measurements, and repetitive sampling of single, localized populations (Brosnahan et al. 2014). Here, we have expanded upon that work through an in situ deployment of an Imaging FlowCytobot (IFCB), a submersible flow cytometer that captures high quality images of phytoplankton 10–100 μm in length at rates up to 12 s^{-1} (Olson and Sosik 2007). An accompanying suite of image analysis and classification software makes it possible to quantify the affinity of images to genus and species-specific classes (Sosik and Olson 2007). The IFCB was deployed in Salt Pond (Eastham, Massachusetts), a small, tidal subembayment within the Nauset Marsh system (NMS; Fig. 1). This site experiences nearly annual, localized blooms of *Alexandrium fundyense*, a toxic *Alexandrium* species that is endemic to North and South America (John et al. 2014). Blooms within the pond are inoculated by local cyst germination and retention of planktonic stages enables observation of their progression through this species' sexual life cycle. *A. fundyense* populations within the NMS are also chronically impacted by intracellular parasites from the genus *Amoebophrya*, a group of small dinoflagellates that are associated with bloom termination, both through direct lysis of host cells and, in some species, through induction of host encystment (Toth et al. 2004; Chambouvet et al. 2011).

During its life cycle, the *Amoebophrya* parasite alternates between a free-swimming, infective stage called a dinospore and a multinuclear, intra-host growth phase called a trophont (Cachon 1969). Dinospores infect new *A. fundyense* hosts through invasion of the host cell's cytosol, then nucleus before transforming into the trophont stage through nuclear division and flagellar replication. Mature trophonts are multinucleate and often displace the contents of the host cell, eventually expanding through the host cell wall to form a short-lived, vermiform that breaks apart into hundreds of new infective dinospores (Fritz and Nass 1992).

Our goals in this study were (1) to develop *A. fundyense* image classifiers for the detection of different life cycle stages and *Amoebophrya* infection, (2) to evaluate the performance of the IFCB and automated image classification for *A. fundyense* bloom monitoring, and (3) to record and characterize a natural *A. fundyense* bloom through its full duration, especially its transition from vegetative cell division to the formation of gametes and planozygotes, and including estimation of daily division rates. The results from these activities are presented here and products from our IFCB image analysis are compared to microscopy-based assessments of *A. fundyense* abundance and *Amoebophrya* infection.

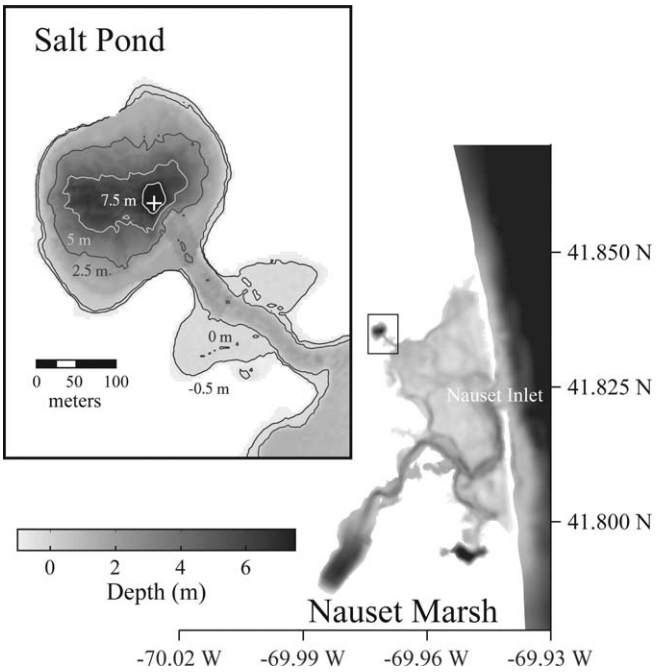

Fig. 1. Bathymetric map of the Nauset Marsh system. A shallow central marsh area connects Salt Pond to the Atlantic Ocean via a narrow inlet while also isolating its *A. fundyense* blooms. Inset: Salt Pond bathymetry. The IFCB support raft was installed near the pond's central hole (marked by white cross).

Materials and methods

Study site

Salt Pond is a drowned kettle pond and the northwestern most extremity of the NMS (Fig. 1). It is approximately 320 m in diameter and has average and maximum depths of 3.4 m and 9 m. Tides are semi-diurnal with a range of 1–1.5 m and short floods relative to ebbs (3–4 h vs. 8–9 h, respectively). Stratification of the water column is maintained via salinity and temperature gradients, although the relative importance of these factors changes seasonally, salinity being the more important driver during winter and early spring when air and water temperatures are similar. Surface salinities near the pond's center are typically 1–2 less than oceanic water advected from Nauset inlet, a gradient produced through freshwater inputs from precipitation, run-off, and groundwater discharge around the pond's perimeter and near its mouth (Crusius et al. 2005). As air temperatures and solar irradiance increase in spring and summer, bottom water within the pond heats more slowly than surface water, leading to gradients sometimes >5°C (Anderson and Stolzenbach 1985; Crespo et al. 2011; Ralston 2015).

Salt Pond is an ideal site for the study of *A. fundyense* because its blooms of *A. fundyense* are "self-seeded" with new vegetative cell populations initiated through the germination of cysts deposited during previous bloom cycles (Crespo et al. 2011). Bloom populations are also retained and isolated

from those occurring in the southern reaches of the NMS and along the coast due to a combination of swimming behavior, the bathymetry of Salt Pond, and water column stratification. Previous observations and a modeling study suggest that these factors increase the residence time of *A. fundyense* cells 1.5–4-fold compared to passive particles, from ~2 d to 3–8 d (Anderson and Stolzenbach 1985; Ralston et al. 2015). Similar retention of blooms in the southern NMS ponds causes advective fluxes of cells in and out of Salt Pond to be low relative to local growth and loss processes (Ralston et al. 2015). In this study, both the development and termination phases of the 2012 *A. fundyense* bloom were therefore identified directly from changes in cell abundance and without consideration of advection in or out of the pond.

Concurrent projects also quantitatively evaluated losses due to parasitism by *Amoebophrya* (Velo-Suárez et al. 2013) and grazing by diverse species (Petitpas et al. 2015), enabling comparisons between the roles of these losses and sexual fusion as contributors to the *A. fundyense* bloom's decline.

Cable-free mooring deployment of the Imaging FlowCytobot

The IFCBs deployed in Salt Pond were second-generation prototypes that incorporated several changes from the original system (described by Olson and Sosik 2007). The purpose of these modifications was to reduce both the size and power consumption of the original IFCB. Changes included the following: (1) replacement of the camera with a new, smaller GigE camera; (2) replacement of the PC104+ computer with a new Intel Atom processor based computer; (3) replacement of the flash lamp module and power supply with a smaller, low-power version; and (4) installation of a custom opto-mechanical system that incorporated a more compact syringe pump and reduced the number of control and data acquisition boards. The updated design is approximately half as heavy, uses 1/3 the power, and is more stable and simpler to operate than the original version. It is also essentially identical to the version that is now commercially available through McLane Research Laboratories (Falmouth, Massachusetts).

The basic functionality of the second generation IFCB and its accompanying software suite is essentially the same as earlier versions that have been deployed for in situ monitoring (Olson and Sosik 2007; Campbell et al. 2010; Peacock et al. 2014). One modification to the instrument software was addition of an alternating acquisition capability that enabled switching between high- and low-sensitivity cell detection modes. This was an effort to record the fullest diversity possible of red fluorescent cells and particles in Salt Pond while also improving the quantitation of *A. fundyense*. The volume of seawater analyzed by the IFCB is inversely related to its triggering rate because the system does not record new images while processing camera data. High sensitivity acquisitions recorded unbiased samples but effective analysis rates were sometimes <5 mL h^{-1}. Low sensitivity acquisitions applied a higher trigger threshold that more specifically targeted chlorophyll-rich cells like *A. fundyense* and typically enabled analysis rates >10 mL h^{-1}.

The IFCB was deployed in Salt Pond at 5 m depth, below a custom built raft that supplied power and an Internet connection. Raft components included a 3000 kW gasoline generator (Yamaha), 10 $LiFePO_4$ batteries and chargers (DeWalt, 790 Wh total capacity), and a PIC microcontroller that monitored battery bank charge status and started the generator as needed (typically 1 h charging per day). The IFCB and PIC microcontroller were connected to the Internet via an Ethernet radio system (FreeWave FGRplus RE) and a DSL connection at the nearby Cape Cod National Seashore Salt Pond Visitor Center. Data bandwidth was adequate to transfer data from the instrument to a shore-based server in near real time while also controlling the IFCB acquisition software. The system consumed about 1/3 gallon gasoline d^{-1} during continuous operation of the IFCB and was refueled every 7–10 d. The raft itself was secured over the deepest area of the pond (8–9 m deep) by three mooring anchors. These anchors both fixed the location of the raft and also prevented tangling of the anchor lines and the IFCB.

The support raft was deployed 15 March and recovered 22 June 2012. One of two prototype IFCBs was deployed during this period except for two gaps (17–20 March and 14–21 May) when maintenance was needed for the installed instrument and the second was unavailable. Additional data gaps occurred due to malfunctions in developmental versions of the IFCB software. In most cases, these malfunctions were detected in less than 1 d and normal sampling resumed after restarting the instrument.

Weekly NMS surveys and other sampling in Salt Pond during the raft deployment

Weekly surveys of NMS physical and biological conditions were conducted during the IFCB deployment as described elsewhere (Crespo et al. 2011; Ralston et al. 2014). These activities are outlined again here with emphasis on data collection within the confines of Salt Pond. An additional, intensive survey of the *A. fundyense* parasite *Amoebophrya* was also conducted (Velo-Suárez et al. 2013) and data from that study were used for comparison to IFCB-based estimates of infection prevalence. NMS surveys coincided with daytime high tides and were begun 14 February and repeated approximately weekly through 8 May, about 2 weeks after the last *A. fundyense* cells were detected by IFCB. Survey stations included one adjacent to the IFCB raft and three around the pond's periphery, one each near the pond's northern, eastern and western shores, but only data from the IFCB raft station were compared directly to the IFCB record. During each survey vertical profiles of salinity and temperature were taken using a Sea-Bird 19plus CTD (Sea-Bird Electronics,

Bellevue, Washington). Niskin bottle samples were taken from depths of 1 m, 3 m, and 5 m and 1 m above the bottom (7–8 m) at the IFCB raft station and at 1 m depth and 1 m above the bottom at the peripheral stations. Subsamples from each bottle were analyzed for *A. fundyense* abundance and nutrient concentrations. Samples from the IFCB raft station (but not peripheral samples) were also analyzed for *Amoebophrya* infection prevalence and *Amoebophrya* dinospore abundance.

A. fundyense were counted after staining with a species-specific fluorescent oligonucleotide probe (NA1; 5′-AGT GCA ACA CTC CCA CCA-3′) as described by Anderson et al. (2005). All nutrient measurements (nitrate + nitrite, ammonium, and phosphate) were made from 0.22 μm filtrates of whole seawater that were collected in sample-rinsed bottles and stored on ice in the field then frozen until analysis at the Atlantic Research and Learning Center Laboratory at Cape Cod National Seashore.

Amoebophrya dinospore and *A. fundyense* host infection prevalence were assessed as described by Velo-Suárez et al. (2013). In addition to samples from weekly surveys, Niskin bottle collections at 1 m, 3 m, and 5 m depths were collected every 1–3 d through the full course of the *A. fundyense* bloom (20 March–8 May). Whole seawater samples were fixed in the field with 2.5% formalin (v/v) and stored on ice until returning to the laboratory where samples were prescreened through 100 μm Nitex mesh then fractionated over 15 μm Nitex mesh. Dinospore (<15 μm) and *A. fundyense* host (>15 μm) fractions were then concentrated on 0.8 and 5.0 μm polycarbonate filters, respectively, and dehydrated through serial washes with 50%, 80%, and 100% ethanol. After washing, filters were dried at room temperature then stored at −20°C until staining with a horseradish peroxidase-coupled oligonucleotide probe (ALV01; 5′-GCC TGC CGT GAA CAC TCT-3′; Chambouvet et al. 2008) using fluorescence in situ hybridization coupled with tyramide signal amplification (FISH-TSA). Individual host infections were graded "early" if detectable as a small dot within the host cell, "intermediate" if an *Amoebophrya* cell cluster was present, and "mature" if the parasite had formed a multinuclear trophont.

Several records of physical conditions at the pond were made with instruments installed during the IFCB raft deployment and at a local environmental monitoring station. Instrumentation included a pair of XR-420 conductivity–temperature loggers (RBR, Kanata, Ontario, Canada) that were hung from the IFCB raft at 1 m and 5 m depths to measure water temperature and salinity above and below the pond pycnocline and a HOBO data logger deployed ~30 m from the southwestern shore of the pond that recorded temperature and water level. Surface irradiance measurements were taken from the Massachusetts Department of Environmental Quality monitoring station in Truro, Massachusetts, approximately 16 km north of Salt Pond.

Image classifier development

Development of Salt Pond-specific image classifiers was undertaken using a suite of publicly available MATLAB-based tools (https://beagle.whoi.edu/svn/ifcb/trunk). These tools create a classification "machine" that compares an image's features (image dimensions, geometry, cell shape, texture, etc.) to those from example image sets defining species- and genus-specific classes. An early version of this software was described by Sosik and Olson (2007) and subsequent development has led to numerous improvements including integration with a web-based interface for data access in standardized formats, interactive browsing of time series images via a web "dashboard" (see http://ifcb-data.whoi.edu/saltpond/), and use of a "random forest" based machine-classification scheme. The random forest approach is a significant improvement over the earlier support vector machine approach: training set images do not need to be withheld for performance assessments, there is no parameter tuning, the machines are insensitive to redundant or low information image features, and there is no risk of over fitting to the training data (Breiman 2001).

Example images of over 60 species and genus-level categories were manually identified through an iterative process that reviewed IFCB images collected at regular intervals over the complete course of the *A. fundyense* bloom (mid-March to early-May). Throughout this process, *A. fundyense* images were given special attention, and additional training sets for several life cycle- and cell number-specific subclasses were created. These training sets included *A. fundyense* singlets, doublets, triplets, and quadruplets; fusing gamete cells; dividing vegetative cells; combinations of singlet, doublet, and triplet cells captured in single images; cells with mature grade *Amoebophrya* infections; and lysed *A. fundyense* singlets (Fig. 2). Classes describing paired cells (dividing vegetative cells, vegetative doublets, and fusing gametes) were differentiated based on the orientation of the constituent cells' cingular grooves (parallel in vegetative cells and oblique in fusing gamete pairs), their relative size (fusing gametes often being unequal), and the length of the cells' contact area. Paired cell images in which these features are obscured were classified as vegetative doublets.

Preliminary Salt Pond random forest classifiers were built using limited sets of training images and then applied to the dataset. The automated classifications were then reviewed to define requirements for new training images. In addition to *A. fundyense*, training classes included other dinoflagellates (*Amylax triacantha*, *Dinophysis acuminata*, *Gyrodinium* sp., *Heterocapsa triquetra*, and *Polykrikos* sp.), diatoms (*Chaetoceros* spp., *Guinardia* spp., *Lauderia* sp., *Leptocylindrus* spp., *Skeletonema* sp., and *Thalassiosira* sp.), and ciliates (*Favella* spp., *Laboea* sp., *Mesodinium* sp., *Strombidium* sp., and other aloricate choreotrich spp. groups). Training set images were sometimes heavily biased toward narrow temporal ranges within the time series, which has the potential to weaken

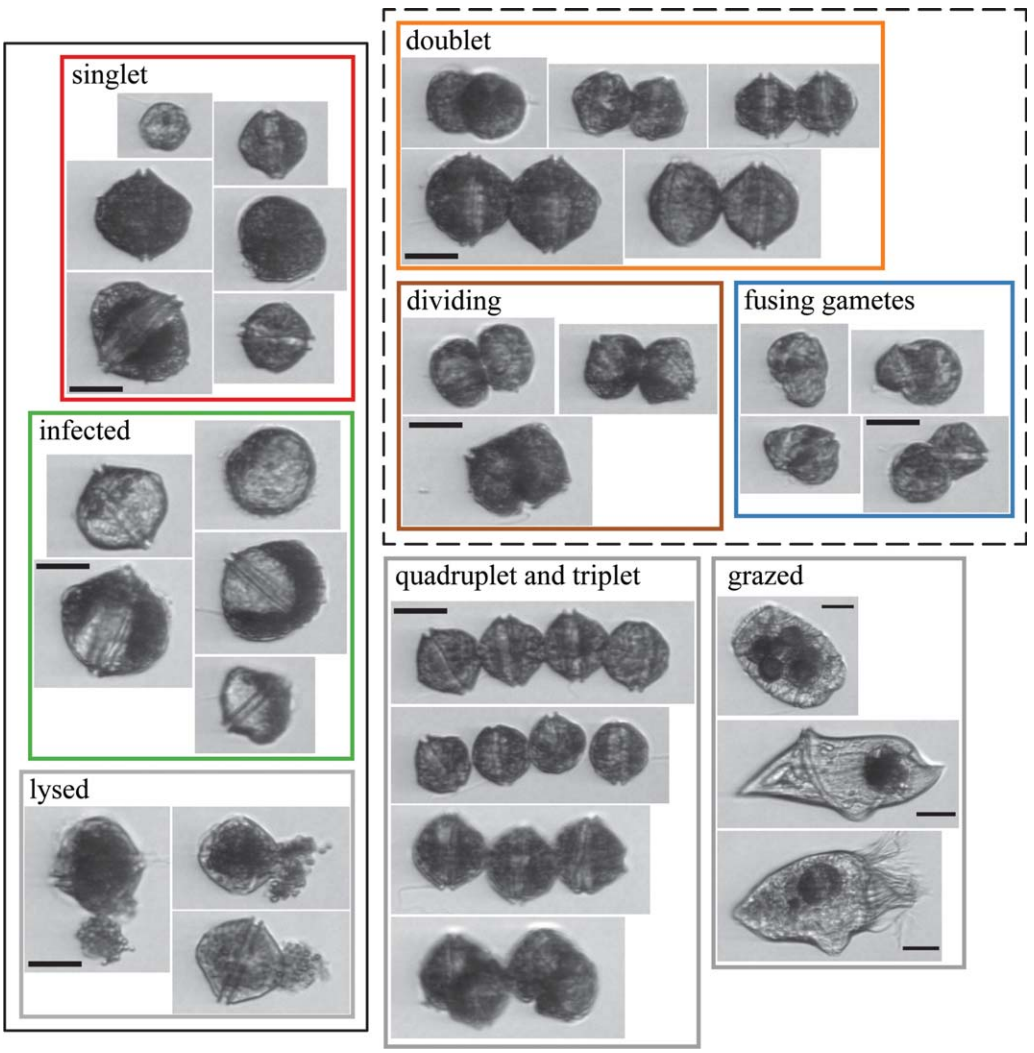

Fig. 2. Example images from a subset of *A. fundyense* subclasses and select grazers. Subclass collages are outlined by colors used in subsequent figures when applicable. Classes lumped together as singlets and doublets in the two *A. fundyense* subclass classifier are bounded by solid and dashed black lines. All scale bars are 25 μm. Examples in the "grazed" collage are from species that were commonly observed to have ingested *A. fundyense* and are identified as *Polykrikos* sp., *Gyrodinium* sp., and an aloricate choreotrich ciliate (top to bottom).

classifier skill against classes that vary in size or morphology with time. Because significant changes in *A. fundyense* singlet size were noted near the bloom's peak and during termination, we drew roughly equal numbers of *A. fundyense* images from three periods in the IFCB record (20 March–13 April, 14–18 April, and 19 April–1 June) whenever possible to construct final versions of the training sets. Classes included in final classifier versions had a minimum of 50 and no more than 400 total images, yielding a total of 11 *A. fundyense*-specific subclasses and 40 classes for other taxa. Three final classifiers were constructed for performance comparisons: one classifying all *A. fundyense* subclasses separately (11-subclass), one lumping all *A. fundyense* subclasses into a single class (1-subclass), and one lumping *A. fundyense* subclasses into singlet and doublet subclasses (2-subclass). Of the complete set of 11 subclasses, "singlet," "*Amoebophrya* infected," and "lysed" subclasses were all counted as singlets in the 2-subclass classifier and "doublet," "fusing gametes," and "dividing" subclasses were all counted as doublets. Images from the remaining five subclasses—"doublet pair," "quadruplet," "singlet and doublet," "singlet pair," and "triplet"—were not included in the 2-subclass training sets.

The performance of the three final classifiers was assessed for (1) sensitivity and specificity for *A. fundyense* (measures of the classifiers' ability to detect *A. fundyense* images and to reject other classes from the *A. fundyense* subclasses), (2) accuracy of total *A. fundyense* cell abundance estimates, and (3) detection of *A. fundyense* singlets across their full size range. The samples examined were drawn from 04:00 to 16:00 h (EDT) IFCB samples at 3-d intervals from 24 March

to 26 April and 0:400, 10:00, 16:00, and 22:00 h, every day from 13 to 20 April.

Sensitivity and specificity were evaluated without regard to whether subclasses were correct because the number and character of the subclasses differed between classifier versions and were defined as:

$$\text{Sensitivity} = \frac{TP}{TP+FP}$$
$$\text{Specificity} = \frac{TN}{TN+FN}$$

where TP, FP, TN, and FN were the number of true positive, false positive, true negative, and false negative images according to whether they were classified as a member of any *A. fundyense* subclass (or not).

For comparison of abundance estimates, counts from the manually corrected, 11-subclass classifications were used as a benchmark because these were the only classifications that accurately counted *A. fundyense* from multi-cell images (doublets, triplets, quadruplets, and combinations of these and singlet cells captured within single *A. fundyense* images).

Assessment of bias across the observed size range in singlet *A. fundyense* subclasses (singlet, *Amoebophrya* infected, and lysed cells) was undertaken because estimates of cell division rate and sexual stage partitioning relied on automated classifications to extract the population's size distribution. Singlet size was evaluated using the IFCB image processing suite's automated biovolume estimator (Moberg and Sosik 2012) and converted from voxels to cubic microns using a conversion factor of 2.66 pixels per micron. After initial assessment showed that the full singlet size range was observed within the period from 13 to 27 April, singlet cell images identified in manually corrected samples from this period were compiled and sorted into 75 volume bins equally spaced along a base-2 log scale ranging from 4096 to 131,072 μm^3 (or $2^{12}-2^{17}$ μm^3). For conciseness, cell volume quantities are hereafter expressed as powers of 2 since 1 unit changes in the exponent indicate twofold changes in cell size (as expected during a cell division).

The miss rate (P_{miss}) for each volume bin and classifier version was calculated by dividing the number of false negatives by the actual number of singlet images (evaluated after lumping vegetative, infected, and lysed singlet classifications). The performance of the three classifier versions was then ranked according to which minimized the volume-dependent variation and overall mean of P_{miss}.

Estimates of accumulation, loss, and cell division

A. fundyense populations in Salt Pond, like other algal blooms, are patchy in their spatial distribution, a characteristic that can complicate comparisons of cell abundance over time, especially if patchiness is a larger source of variance than population-level changes associated with its temporal evolution. Therefore, mean estimates of overall abundance recorded during weekly surveys and abundance at each survey sampling station were compared with the IFCB record to assess whether the dates when the bloom transitioned from development to decline were consistent. Abundance estimates from 1 m (the only depth sampled at all four stations within the pond) were also analyzed by ANOVA to assess the relative contributions of survey date (temporal evolution) and station (sampling location) to differences in cell abundance.

A. fundyense cells migrate vertically through the water column, forming layers at depths of 2–3 m during the day, then 4–6 m at night (Anderson and Stolzenbach 1985), introducing an additional source of variability in the abundance estimates. Vertical migration caused strong diel oscillations in cell concentration at the IFCB that were superimposed over shorter time scale variability associated with spatial patchiness. The strength of the diel pattern was assessed through a Lomb–Scargle spectral analysis of IFCB-based abundance estimates ($p \ll 0.001$), which was consistent with overnight aggregation of cells near the IFCB sampling port (5 m). To minimize effects of patchiness, accumulation and loss from the population were calculated from changes in mean overnight concentration of IFCB-based abundance estimates (typically 18 samples taken from 21:00 to 03:00 h each night). Specific rates of net accumulation (or loss when < 0) were denoted μ_{net} and calculated as:

$$\mu_{\text{net}} = \frac{\ln(\bar{C}_t/\bar{C}_0)}{t}$$

where $\bar{C}_t$ and $\bar{C}_0$ are the overnight means on nights separated by t days. Importantly, estimates of μ_{net} combined several population growth and loss factors including germination, cell division, grazing, parasitic lysis, sexual fusion, encystment, and advective processes.

In parallel, IFCB images of *A. fundyense* were also used to estimate daily rates of cell division by comparing mean cell volume before and after the population underwent phased division (DuRand and Olson 1998). Estimates of the cell division rate relied on the identity:

$$\frac{N_{\text{divided}}}{N_{\text{undiv.}}} = \frac{\bar{V}_{\text{undiv.}}}{\bar{V}_{\text{divided}}}$$

where $N_{\text{undiv.}}$ and N_{divided} are the number of cells before and after the Salt Pond population underwent a phased division and $\bar{V}_{\text{undiv.}}$ and $\bar{V}_{\text{divided}}$ are the mean cell volumes of those populations. $\bar{V}_{\text{undiv.}}$ and $\bar{V}_{\text{divided}}$ were determined from a 2-h moving time average of singlet volume that maximized daily volume shifts within a period of 12 h. The restriction to singlet images was necessary because volumes from multi-cell images were often grossly underestimated due to rotation of chained cells out of the plane of focus. Note that the enumeration of these forms was not similarly compromised. Under the assumptions that (1) all divisions are phased and (2) that there is no growth in the population's total

biovolume during the division period, estimates of the specific daily division rate were calculated as:

$$\mu_{\mathrm{div}} = \ln\left(\frac{\bar{V}_{\mathrm{undiv.}}}{\bar{V}_{\mathrm{divided}}}\right)$$

The μ_{div} expression provides a minimum estimate of division rate since it underestimates to the extent that assumptions (1) and (2) are violated. The restriction to singlet images further underestimates μ_{div} because chained cells (doublets, triplets, and quadruplets) are younger (and therefore their constituent cells smaller) on average than singlets, causing overestimation of $\bar{V}_{\mathrm{divided}}$. An additional and uncontrolled source of error is the potential for size distribution bias between pre- and post-mitotic periods as *A. fundyense* singlets swam toward the surface (and away from the IFCB) during their morning migration to shallower depth.

DNA content analysis

DNA content of *A. fundyense* cells collected during weekly surveys was assessed to measure the proportion of planozygotes and post-replication vegetative cells (i.e., those in the G2 and M phases of the cell cycle). Both planozygotes and G2+M phase vegetative cells have 2c DNA content or approximately twice the typical DNA content of haploid, G1 phase vegetative cells (Brosnahan et al. 2014; McGillicuddy et al. 2014).

Subsamples for DNA analysis were taken from seawater concentrates produced through our standard *A. fundyense* counting procedure (described above; Anderson et al. 2005). The DNA analysis presented here was limited to samples collected at the raft from periods when *A. fundyense* were dominant (3, 10, 17, and 24 April) and to depths where concentrations were $>20{,}000$ cells L^{-1}. Subsamples contained approximately 10,000 *A. fundyense* cells and were stained with propidium iodide (PI) for analysis with a FACSCalibur flow cytometer (BD Biosciences) as described by McGillicuddy et al. (2014). Because surveys could only be completed during daytime high tides, the time of day when samples were collected varied but was always between mid-day and mid-afternoon when most vegetative cells are typically in the G1 phase of the mitotic cycle. Although the instrument and sample preparation used could not unambiguously identify individual *A. fundyense* during analysis, the approach is relatively insensitive to staining variability associated with the duration of formalin fixation in the field (Brosnahan et al. 2014). *A. fundyense* singlet populations were readily identifiable via a series of forward scattering, side scattering, and PI fluorescence gates because they have extraordinarily high DNA content per cell and were dominant in the samples analyzed.

PI fluorescence was recorded from 700 to 1200 *A. fundyense* cells per sample using CellQuest Pro software version 5.2.1 on a Macintosh computer running operating system version OSX 10.4.11. Acquisition scaling of PI fluorescence was set to linear with voltage and threshold settings adjusted to capture the complete distribution of 1c–4c *A. fundyense* cells. All other light scattering and fluorescence parameters were acquired with logarithmic scaling. System and sample stability were assessed through analysis of a culture control immediately before and after analysis of the field samples. To identify and compare the relative abundance of DNA content populations, data were imported to MATLAB and analyzed using mmvn_toolkit for Gaussian mixture modeling (GMM; Boedigheimer and Ferbas 2008).

Continuous culture experiment

A continuous culture of *A. fundyense* was established and monitored by an IFCB under light and temperature conditions similar to those observed during the peak of the Salt Pond *A. fundyense* bloom. The purpose of this experiment was to evaluate IFCB-based estimates of infection and cell division under laboratory-controlled conditions and also to explore behavioral differences between a clonal culture and the Salt Pond population.

A 1-L culture of clone ATSPF7-5 was grown in a glass water-jacketed flask with light supplied by a combination of fluorescent and tungsten-halogen bulbs. Culture lights were turned on and off in a stepped fashion to approximate the light: dark cycle experienced by vertically migrating *A. fundyense* field populations (Anderson and Stolzenbach 1985; Brosnahan and Ralston unpubl.). The overall light period was approximately 12 h long including two, 2-h long, four-step ramps between darkness and peak light intensity. Irradiance within the flask under full light was measured with a QSL-100 wand-type radiometer (Biospherical Instruments) and ranged from 325 μmol photons m^{-2} s^{-1} to 540 μmol photons m^{-2} s^{-1}. The uninfected culture was sampled hourly by an IFCB that was configured to replace samples with an equal volume of nutrient-replete medium. The medium was prepared essentially as f/2 minus silicate (Guillard and Ryther 1962) but modified through addition of 10^{-8} mol L^{-1} H_2Se0_3 and by reduction of $CuS0_4$ to 10^{-8} mol L^{-1}. Vineyard Sound seawater (0.2-μm filtered, salinity $\sim$31) was used as the medium base. Prior to sampling, the culture was mixed gently by a caged magnetic stir bar (approximately 6 min each hour). Temperature within the culture oscillated between 10.2°C (culture night) and 10.8°C (culture day) due to heating from its lamps. From a prior experiment it was known that ATSPF7-5 divides with a specific growth rate of $\sim$0.2 d^{-1} under these conditions. Therefore the hourly sample/replacement volume was set to 8.5 mL h^{-1} (204 mL d^{-1}), which approximately balanced growth and dilution. Cell concentrations were monitored for 6 d to ensure that cells were dividing normally before the culture was infected with free-swimming *Amoebophrya* dinospore cells.

A 300-mL inoculum of *Amoebophrya* was prepared in a 12°C incubator using ATSPF7-5 as its host. Dinospores ($\sim$3

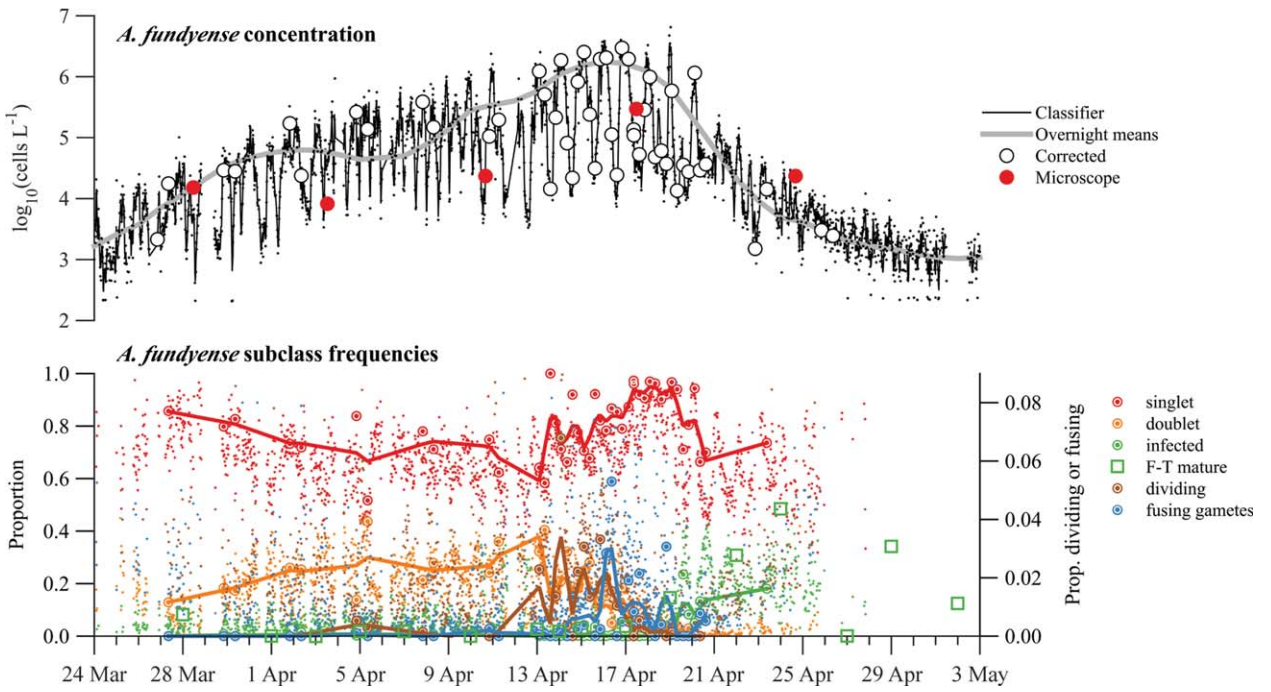

Fig. 3. (Top axes) Abundance estimates derived from the two *A. fundyense* subclass machine classifier. Lines are loess smoothing results from sample estimates. Classifier data (fine black points) are estimates taken directly from the 2-subclass classifier output. Overnight means are derived from observations collected between 21:00 and 03:00 h EDT when *A. fundyense* were concentrated near the IFCB intake. Corrected data are abundance estimates from manually corrected IFCB samples. Microscope data are abundance estimates from weekly surveys (Bottom axes) Select *A. fundyense* subclass frequencies. Large ringed circles are manually corrected estimates from IFCB images and fine points are results from the 11-subclass machine classifier. Lines are loess smoothing results from manually corrected data. Fusing gametes and dividing vegetative cells were never greater than 5% of *A. fundyense* images within a single sample and are plotted against the right *y*-axis. Open square symbols are FISH-TSA-based estimates of mature *Amoebophrya* infection prevalence.

μm in diameter) were separated from their infected host culture by filtering through a 20 μm Nitex sieve. The volume of the continuous culture was reduced by 300 mL immediately prior to inoculation with a pipette whose end had been covered by 20 μm Nitex mesh. After inoculation, the culture was mixed approximately 2 min by magnetic stir bar before triplicate, 1-mL samples were collected to estimate the initial concentration of dinospores. Samples were fixed with 2.5% (v/v) formalin and stored in a refrigerator (4°C) 10–14 h. Following fixation, samples were concentrated on 0.8 μm polycarbonate filters and prepared for FISH-TSA staining as described for *Amoebophrya* field sampling. The frequency of IFCB sampling was also reduced to 8 d^{-1} (sampling every 3 h) because exposure of the culture to *Amoebophrya* was expected to arrest cell division, leading to excessive dilution. Additional FISH-TSA samples were taken approximately 1 h after culture daybreak and 1 h before nightfall for 10 d post infection. The IFCB continued sampling every 3 h throughout the infection period but images collected at one sampling point in the third day after infection and from late in 7^{th} day after infection until the end of the experiment were unusable due to obstructions in the instrument's flow cell that compromised cell detection and image focus.

Results

Image classifier assessments

All three of the final classifiers described similar temporal trends in the abundance of *A. fundyense* in Salt Pond, including short-term diel oscillations due to vertical migration and longer-term phases of increasing (bloom development) and decreasing (termination) overnight cell concentrations (Fig. 3). This concordance between the versions reflected similarly excellent specificity (discrimination of *A. fundyense* from other organisms) throughout the bloom's full duration (mean values between 0.995 and 0.997; Fig. 4). Differences among the classifiers included their ability to accurately account for multi-cell images (e.g., doublets), their sensitivity for *A. fundyense*, and their bias across the observed range in *A. fundyense* singlet size.

Like specificity, the sensitivity (ability to detect *A. fundyense* images) of the three classifiers was high on average but the classifiers were consistently ranked such that the sensitivity of the 2-subclass version was greater than the 1-subclass version, and both were greater than the 11-subclass version (mean values 0.865, 0.812, and 0.705, respectively). Lowest sensitivities for each of the classifier versions were clustered in time, occurring between 16 and 24 April (Fig. 4), a period that coincided

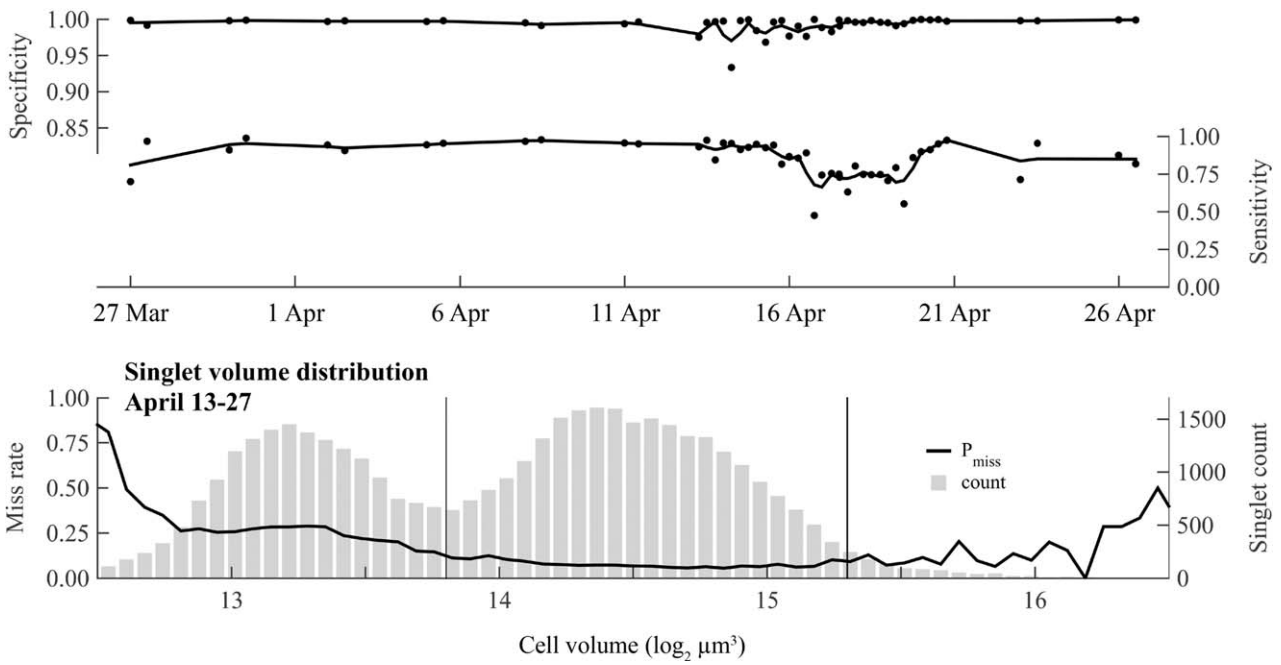

Fig. 4. (Top and middle axes) Specificity and sensitivity of the 2-subclass version of the machine classifier through the full course of the 2012 Salt Pond bloom. Only results from the 2-subclass machine are presented because it is the only version used in subsequent analyses that rely on machine classification. (Bottom axes) Size bias of the 2-subclass version observed in detection of singlet images collected during the transition from bloom development to termination. Counts (gray bars) indicate the relative abundance of different *A. fundyense* size classes (volume bins).

with a marked sexual transition by the bloom (Fig. 3). The lowest sensitivities produced by the 11-subclass version somewhat undermined its unique strength as the only version constructed to discriminate between several life cycle stages.

Classifier-derived estimates of overall *A. fundyense* abundance were well correlated with corrected 11-subclass counts for each of the classifier versions ($R^2 = 0.932$, 0.993, and 0.943 for the 1-, 2- and 11-subclass versions, respectively; Fig. 5). The four most abundant subclasses—singlets, doublets, infected cells, and lysed cells—accounted for greater than 90% of all samples' *A. fundyense* images in the Salt Pond record (Fig. 3). The 2-subclass version's highest skill ranking reflects both its accurate counting of cells from these highly abundant subclasses and its comparatively high overall sensitivity for *A. fundyense*, while weaker performances by the 1- and 11-subclass versions occurred for different reasons. The 1-subclass version did not account for doublets, which were frequently >20% of *A. fundyense* during bloom development (Fig. 3). The 11-subclass version exhibited high error rates among the other scarcer, non-singlet and non-doublet subclasses (e.g., triplet, quadruplet, dividing, and fusing gamete cells), making direct interpretation of automated, rare subclass classifications doubtful. Because of the scarcity of these rarer subclasses, temporal patterns were hard to interpret even in corrected samples. Notable exceptions to these generalizations were the dividing cell and fusing gamete subclasses, whose frequencies surged sequentially near the onset of bloom termination (Fig. 3).

The last assessment of the three classifiers examined their relative bias across the full size range of *A. fundyense* during the bloom's gametic and termination phases. This set of samples was taken between 13 and 27 April, the period when sensitivities were lowest and when two marked shifts in the *A. fundyense* population's mean cell volume occurred (Fig. 6). Performance by the classifier versions in this assessment primarily differed across cell volumes $< 2^{13.8}$ μm^3, a size class that was only abundant at the bloom's peak and is presumed to be gametes (cells within this class were the only ones observed as fusing pairs). The 2-subclass classifier also performed best in terms of size bias, producing P_{miss} values that were always < 0.29 for gametes within one standard deviation of the mean gamete size (volumes between 2^{13} and $2^{13.5}$ μm^3; Fig. 4). In comparison, P_{miss} values from both the 1- and 11-subclass classifiers were > 0.45 across the same gamete size range. P_{miss} values from the 2-subclass version still varied across the full range of cell sizes observed and were higher for smaller (gamete) cells than for larger ones; P_{miss} was always < 0.11 across volumes within one standard deviation of the larger size class cells' mean volume (2^{14}–2^{15} μm^3). This behavior may have skewed estimated cell volume distributions of *A. fundyense* toward larger cell sizes during the bloom's termination phase.

Across all the assessed criteria, the 2-subclass classifier produced the most favorable results and was therefore used as the basis for subsequent analyses that relied on machine-based classifications. Results from the 11-subclass model were also retained because these were the starting point for

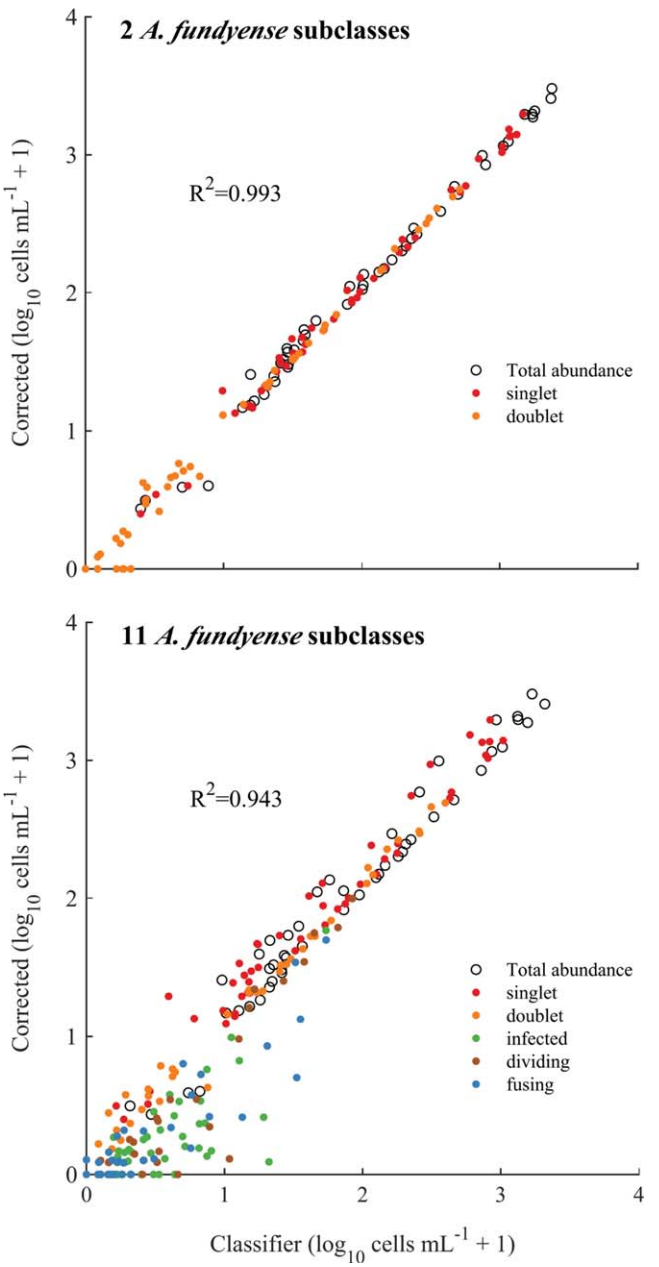

Fig. 5. Comparisons of abundance estimates from 2- and 11-subclass versions of the machine classifier with manually corrected counts that accounted for multi-cell images.

manual correction of the samples that underlie our examination of shifts in the frequencies of different life cycle stage subclasses (which hereafter are limited to dividing cells, fusing gametes and infected cells).

Comparison of IFCB and microscopy-based estimates of *A. fundyense* abundance and infection prevalence

Comparisons of counts from the IFCB and Niskin samples taken adjacent to it showed that the two records were consistent with one another. There was no significant difference between Niskin-based abundance estimates and the mean of IFCB-based estimates collected within 1 h of the bottle samples. Correlation between these records was somewhat weak, however, ($R^2 = 0.63$), a result that reflects both the patchiness of *A. fundyense* within the pond and also uncertainty in the Niskin-based estimates due to subsampling and lack of replication.

Comparison of IFCB-derived and FISH-TSA-based estimates of *Amoebophrya* infection were less affected by patchiness, probably because the quantities compared were proportions. Daily means of the IFCB-estimated prevalence of infection were well correlated with the FISH-TSA derived estimates of mature grade infections ($R^2 = 0.73$) and their differences were not statistically different from zero. The result was further supported by a similar analysis of the continuous culture that compared simultaneous FISH-TSA and IFCB samples (Fig. 7). Again, the estimators were well correlated ($R^2 = 0.84$) and there was no evidence of systematic error between IFCB- and FISH-TSA-based estimates of mature grade infection prevalence.

Accumulation, loss, and cell division rate estimates during three distinct bloom phases

Both the IFCB- and survey-based descriptions of *A. fundyense* abundance in Salt Pond showed distinct development and termination bloom phases, with cells accumulating in the pond from late March through mid-April, then dissipating rapidly (Fig. 3). Spatial patchiness, although readily apparent, did not obscure this temporal pattern.

The peak overnight concentration observed by IFCB occurred 16 April (1.9×10^6 cell L^{-1}), approximately midway between Niskin-based surveys on 12 and 19 April. The maximum Niskin-based estimate of *A. fundyense* abundance occurred during the latter survey when the mean overall concentration reached 8.37×10^4 cells L^{-1}. Maximum station concentrations were split between the 12 and 19 April surveys, with peak mean concentrations at the north and west stations 12 April (5912 and 7325 cells L^{-1}, respectively) and at the east and raft stations 19 April (2.03×10^5 and 1.04×10^5 cells L^{-1}, respectively). Although concentrations sometimes varied by more than two orders of magnitude within individual surveys, only survey day, not station, had a significant effect on abundance at 1 m (survey day: $F_{4,12} = 27.22$, $p \ll 0.001$; station: $F_{3,12} = 0.28$, $p = 0.84$). From these results, and because the IFCB images indicated concerted life cycle transitions, the IFCB record was considered the more precise estimator of *A. fundyense* bloom dynamics.

From analysis of the IFCB images, the mean overnight biovolume of *A. fundyense*, like cell concentration, reached its maximum on 16 April (33 mm^3 L^{-1}; Fig. 6). The development and termination phases of the bloom were therefore identified as the periods before and after 16 April. The bloom's termination was split further into gametic and

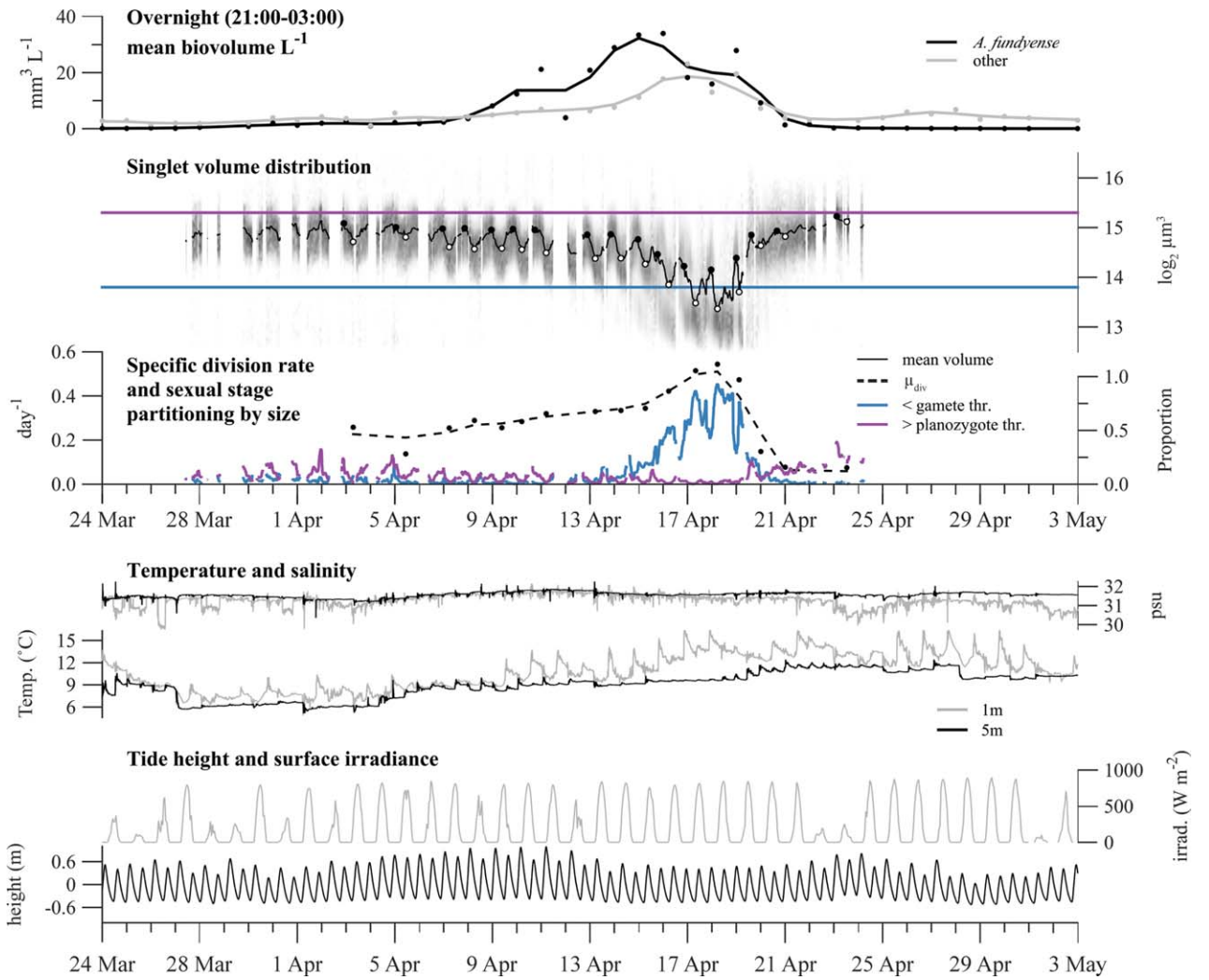

Fig. 6. (Top axes) Total biovolume concentration estimates of *A. fundyense* and all other image classes in Salt Pond. Estimates are calculated during nighttime hours when *A. fundyense* were concentrated near the IFCB. The biovolume of the other classes was calculated from high sensitivity acquisition mode samples only. (Second axes from top) The cell volume distribution is presented as a grayscale histogram at each sample time. The 2-h moving window mean cell volume is overlaid (black line) and its daily minimum and maximum values are highlighted by white and black circles. Thresholds defining "gamete" and "planozygote" size thresholds are drawn in blue and purple, respectively. (Third axes from top) Estimates of the specific rate of division (μ_{div}, calculated from daily changes in mean cell volume, left *y*-axis) and partitioning of *A. fundyense* into sexual stage size classes (right *y*-axis). (Fourth axes from top) Water temperature (left *y*-axis) and salinity (right *y*-axis) measured at 1 m and 5 m depths. Pycnoclines within the pond are typically between 1 m and 2 m deep when present. (Fifth axes from top) Tide height (left *y*-axis) and surface irradiance recorded 16 km north of Salt Pond (right *y*-axis).

zygotic phases based on an assessment of cell volume dynamics through the full course of the bloom.

In the development phase, *A. fundyense* accumulated nearly monotonically from the time the IFCB was deployed (15 March) to the bloom's peak. The mean μ_{net} through this period was 0.30 although this rate varied dramatically when assessed at daily intervals. The most rapid accumulation (0.37 d^{-1}) occurred 5 to 16 April, a period that immediately followed a slow 3-day decline in overnight concentrations. Both the mean cell volume of *A. fundyense* and the doublet frequency exhibited pronounced diel oscillations throughout the development phase, which indicated a high proportion of cells undergoing phased, asexual division. The specific division rate, μ_{div}, was calculated for each day when 2-h moving averages could be drawn from a minimum of 30 singlet images through the division period (typically between 22:00 and 10:00 h). Estimates of μ_{div} were much less variable day-to-day than μ_{net} and increased from approximately 0.21 to 0.42 d^{-1} from 3 to 16 April (Fig. 6). The mean of μ_{div} estimates during the development phase was 0.30 d^{-1}, higher than the mean μ_{net} of 0.24 d^{-1} for the same subset of days.

The transition to bloom decline (termination phase) was marked by a sharp, twofold decrease in cell volume that was sustained for 3–4 d before the size distribution shifted back

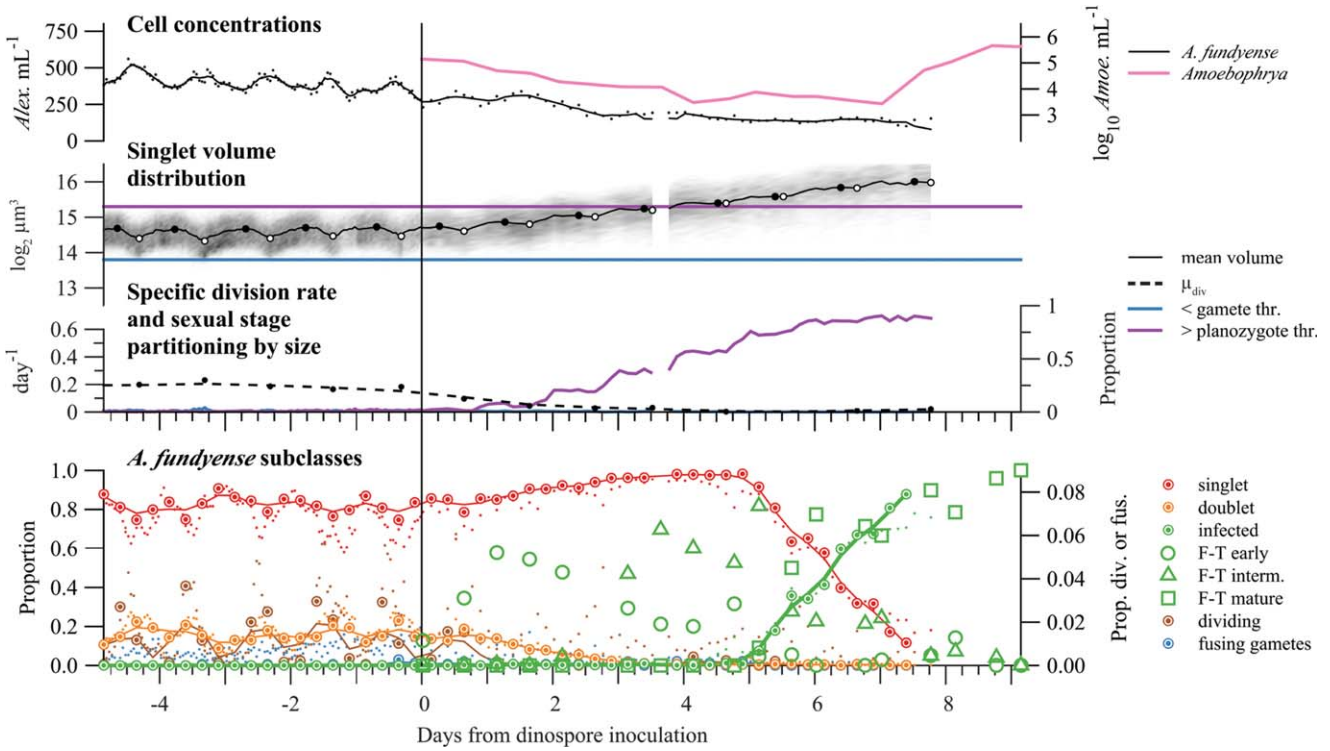

Fig. 7. (Top axes) Concentrations of *A. fundyense* clone ATSPF7-5 (left *y*-axis) and *Amoebophrya* sp. dinospores (right *y*-axis) from a continuous culture experiment. *Amoebophrya* dinospores were inoculated into the culture at Day 0. (Second axes from top) The cell volume distribution is presented as a grayscale histogram at each sample time. The 2-h moving window mean of *A. fundyense* cell volume is overlaid (black line) and its daily minimum and maximum values are highlighted by white and black circles. Thresholds used to define gamete and planozygote size classes in the Salt Pond time series are drawn in blue and purple. (Third axes from top) Estimates of the specific cell division rate (calculated from daily changes in mean cell volume, left *y*-axis) and partitioning of ATSPF7-5 into size classes used to define sexual stages during the Salt Pond bloom (right *y*-axis). (Bottom axes) Select *A. fundyense* subclass frequencies. Large ringed circles are manually corrected estimates from IFCB images and fine points are results from the 11-subclass machine classifier. Lines are loess smoothing results from manually corrected data. Fusing gametes were extremely rare but are plotted for comparison to Fig. 3. Open circles (dotted line), triangles (dash-dot line), and squares (dashed line) are FISH-TSA-based estimates of early, intermediate, and mature *Amoebophrya* infection prevalence, respectively. The smoothed line from IFCB-based estimation of infection rate is bolded to emphasize its similarity to mature grade infection rate estimated by FISH-TSA.

to its development phase range (Fig. 6). The small cells are presumed to be gametes because only cells in this size range were observed fusing; the initial interval within the termination phase is therefore considered a gametic phase. Similarly, the later period of the bloom's termination is presumed to be a zygotic phase since small cells were no longer present and indicators of active division (doublets, oscillating mean cell volume) were absent in spite of otherwise favorable conditions for growth. Throughout the bloom period, the concentration of dissolved inorganic nitrogen was consistently >3 μM and N : P ratios were always <10. Toxic levels of ammonium (>50 μM) were also never observed.

During the gametic phase (16–19 April), overnight cell concentration declined at a rate of -0.33 d^{-1} in spite of a sharp increase in the population's estimated rate of division (μ_{div}: 0.51 d^{-1}, 0.54 d^{-1}, and 0.47 d^{-1}). Doublet frequency, like cell concentration and mean cell volume, continued to oscillate on a diel cycle, but the overall frequency of doublets declined steadily to about 1% of cells by 20 April (Fig. 3). During the subsequent zygotic phase, the population all but ceased its previous diel oscillations in mean cell volume and abundance, indicating a cessation of both cell division and diel vertical migration. Estimates of μ_{div} fell to below 0.1 d^{-1} and the specific rate *A. fundyense* loss (μ_{net}) increased dramatically to -1.0 d^{-1}.

Partitioning of *A. fundyense* into sexual stage-linked size classes

Given that small *A. fundyense* were the only cells observed to undergo sexual fusion, the compilation of all *A. fundyense* images from the bloom's sexual transition (13–27 April; Fig. 4) was used to define a threshold separating gametes from other *A. fundyense* cells. The transition period included the last 3 d of the bloom's development phase and all of its gametic and zygotic phases. The distribution of cell volumes collected from this period was bimodal with peak gamete and vegetative cell/zygote frequencies at approximate volumes of $2^{13.2}$ and $2^{14.35}$ μm^3 (Fig. 4). *A. fundyense* falling

Table 1. Summary from DNA content analysis of samples collected from the IFCB support raft during weekly NMS surveys. Only depths where *A. fundyense* concentrations were greater than 20,000 cells L^{-1} were analyzed. The proportion of 2c cells reported from 17 April is adjusted according to differences in cell abundance between depths. Projected μ_{div} values are calculated under the assumption that all 2c cells will divide during the next phased division and are compared to estimates of μ_{div} from comparisons of mean cell volume ($\bar{V}$) before and after phased division the same day the DNA content sample was taken.

Date (Time)	Depth (m)	1c	2c	Clumped	Proportion 2c	Projected μ_{div} (d^{-1})	μ_{div} from $\bar{V}$ (d^{-1})
03 Apr (12:46)	7	0.67	0.31	0.02	0.316	0.27	0.26
10 Apr (16:06)	5	0.58	0.32	0.10	0.356	0.30	0.28
17 Apr (11:32)	1	0.34	0.61	0.05	0.405	0.34	0.51
	3	0.30	0.61	0.09			
	5	0.61	0.35	0.04			
	7	0.66	0.28	0.06			
24 Apr (16:11)	1	–	–	–	–	–	–
	5	–	–	–	–	–	–

below the local minimum between these modes ($2^{13.8}$ μm^3) were classified as gametes and changes in their abundance were examined over the full course of the Salt Pond time series (Fig. 6). Gametes were occasionally present but never abundant during the early and middle stages of development, typically $<5\%$ of all *A. fundyense* and only present near dawn when cells were dividing. Beginning 14 April, gamete abundance rose rapidly, reaching a peak proportion of $>90\%$ of *A. fundyense* cells during the morning of 18 April. Gamete abundance then fell precipitously, much faster than the overall abundance of *A. fundyense*, and was never greater than 2% of the population after 21 April.

Because past investigations have also classified cells as planozygotes based on cell size (e.g., Anderson et al. 1983; Brosnahan et al. 2014), singlet cells that exceeded a size threshold comparable to the one used in these earlier studies were also tracked. Here, the size threshold used was a volume of $2^{15.3}$ μm^3, which translates to an approximate mean diameter of 42.5 μm. Development phase cells frequently exceeded this threshold, especially at night when some cells were poised to divide. For this reason the proportion of cells presumed to have been planozygotes in earlier studies actually declined as the bloom transitioned from development to the gametic phase of termination. The proportion of large cells then rose steadily during the zygotic phase of the bloom, reaching a peak proportion of 39.4% on 23 April.

DNA content analysis

Because the remaining volumes from the weekly survey samples were limited after cell counting, the number of samples analyzed for DNA content was limited to 5 m and 7 m samples collected 3 and 10 April, respectively (the bloom's development phase); 1 m, 3 m, 5 m, and 7 m samples collected 17 April (gametic phase); and 1 m and 5 m samples collected 24 April (zygotic phase; Table 1). DNA content distributions from the development phase days (single depths) are presumed to be representative of the whole population because they are taken from where cell concentrations were highest. GMM analysis to define 1c and 2c populations was completed interactively but all samples from 3, 10, and 17 April (bloom development through the gametic phase) were effectively modeled as three populations −1c, 2c and "clumped cells"—using "inclusion" type and "most likely" method parameters for gating. No combination of GMM parameters was able to identify distinct populations in samples collected 24 April (zygotic phase), which were heavily impacted by *Amoebophrya* and therefore difficult to interpret (Brosnahan et al. 2014). Approximately one third of cells in development phase samples were 2c, similar to cells at 5 m and 7 m samples during the gametic phase. Proportions of 2c cells were about twice as high in the shallower, 1 m and 3 m depth samples from the gametic phase (Table 1).

Another conservative estimate of μ_{div} can be calculated from these data under the assumption that all 2c cells are set to divide during the next phased division. Estimates of μ_{div} from the two development phase samples were 0.27 d^{-1} and 0.30 d^{-1} for 3 and 10 April, respectively. Notably, both are essentially the same as cell volume-based estimates calculated the same day. Alternatively, the 2c cells recorded in the weekly survey samples might have been set to undergo unphased division. If instead all divided before the next day's phased division, cell volume-based calculations of μ_{div} underestimated the true division rate by about 50%.

The especially high 2c proportions at shallower depths during the gametic phase might be considered evidence of new zygote formation near the surface since they suggest a growth rate outside the conventionally understood envelope of *A. fundyense* cells at any temperature (see Stock et al. 2005 and references therein). However, when controlling for the observed vertical cell distribution, the 2c proportion is much lower (0.405). If all 2c were to undergo division the next morning, μ_{div} would be 0.34 d^{-1}, comparable to the cell

volume-based estimates of μ_{div} during the earlier development period but substantially less than those from the gametic phase of the bloom ($\sim$0.5 d^{-1}).

Continuous culture

Analysis of the continuous culture considered two phases of the experiment: an initial high dilution rate assessment of cell volume-based μ_{div} estimation in uninfected culture, then a low dilution rate assessment of an *Amoebophrya* infection (Fig. 7), both under temperature and irradiance conditions comparable to those experienced by *A. fundyense* 14–16 April, near the peak of the Salt Pond bloom (Fig. 6).

In the initial high dilution rate phase, ATSPF7-5 growth compensated for dilution and concentration remained near its inoculum level (350–525 cells mL^{-1}; Fig. 7). Phasing of division was essentially complete, with minimums in mean volume occurring simultaneous with exposure to full light intensity each day (2 h after culture daybreak). Dividing cells were detected throughout the pre-infection period, oscillating from 1% to 4% during culture night and falling to $<0.5\%$ during culture day. The mean of μ_{div} estimates was 0.193 d^{-1}, which was similar to the culture's dilution rate (0.204 d^{-1}). This growth rate was also indistinguishable from results of batch cultures of ATSPF7-5 that examined growth response to a temperature gradient under high light (>400 $\mu E\ m^{-2}\ s^{-1}$) and a 14: 10 light: dark cycle (typical light conditions for assessing maximal growth in culture; data not shown). With regard to the continuous culture's size distribution, cells were rarely outside the range specified by the gamete and mature planozygote thresholds used to classify sexual stages in the Salt Pond time series (<5% for all time points).

The inoculum of *Amoebophrya* dinospores at the start of the slow dilution phase was one third greater than that observed at any point during the Salt Pond bloom (>300 dinospores/*A. fundyense* host in culture compared to a maximum of $\sim$200 dinospores/host in Salt Pond; Velo-Suárez et al. 2013). Dinospore abundance declined steadily through the first week of the infection (-0.49 d^{-1} after subtracting losses from dilution).

A. fundyense division rate declined immediately on exposure to *Amoebophrya* and divisions were not apparent 2 d after infection. A subsequent decline in *A. fundyense* concentrations could be explained by dilution until the end of the experiment. The difference in loss rates between *A. fundyense* and *Amoebophrya* is attributed to new infections, which were detected within minutes of inoculation (Fig. 7). Early stage infections detected by FISH-TSA reached their peak just 1 d into the experiment and subsequent peaks in intermediate and mature stage infections followed 3 and 6 d later. Multiple infections were common (about 75% of all infections observed 1 d after inoculation with dinospores) with some host *A. fundyense* infected by five or more *Amoebophrya*. Seven days after the initial infection, lysed *A. fundyense* became increasingly abundant (not shown) and *Amoebophrya* dinospore concentration increased dramatically (>5000-fold). A gap in the IFCB record then occurred because a blockage in the system's flow cell made its images unusable. The system continued to exchange culture and media but its imaging was not corrected until effectively all remaining *A. fundyense* cells were lysed (10 d post infection).

Estimates of the duration of each *Amoebophrya*-infection stage—2 d, 3 d, and 1 d for early, intermediate, and mature stages, respectively—were made by comparing the timing of peaks in each stage's abundance and the pulse of new dinospores. The sum of these (6 d) is slightly longer than was observed in Salt Pond (4–5 d; Velo-Suárez et al. 2013). Exposure to *Amoebophrya* did not cause ATSPF7-5 to produce gamete-sized cells or promote fusion, nor were any cysts recovered at the end of the experiment. Instead, ATSPF7-5 grew steadily larger with the cessation of cell division, such that essentially all *A. fundyense* exceeded the planozygote threshold 7 d after the introduction of dinospores (Fig. 7).

Discussion

The approach described here directly addressed three longstanding challenges in studies of sexual transitions by natural marine phytoplankton blooms: (1) the difficulty of making detailed and high frequency observations, (2) the need to sustain high frequency sampling for extended periods (more than 1 month), and (3) the need to follow single populations. The IFCB—an automated imaging instrument that was purposefully designed for long term, in situ deployments—was invaluable for addressing the first two of these challenges. Our approach to the third challenge was made possible through the development of a cable-free raft that supported the IFCB deployment at Salt Pond, a site that retains *A. fundyense* blooms and can be adequately characterized by sampling at a single location and depth. Deployment at Salt Pond also enabled comparison to weekly surveys of *A. fundyense* that were ongoing through other parallel projects within the NMS (Velo-Suárez et al. 2013; Ralston et al. 2014, 2015; Petitpas et al. 2015).

Comparison of the IFCB time series to data collected during weekly surveys of *A. fundyense* abundance (and sometimes daily estimates of *Amoebophrya* infection) showed reasonable correlations and no bias between sampling methods. The most obvious difference between the datasets was the lack of temporal, physiological and ecological richness from weekly surveys compared to the IFCB record. One exception to this generalization was the sometimes daily record of *Amoebophrya* dinospores and host infections from FISH-TSA analysis since only the FISH-TSA approach characterized the dynamics of the free-swimming and early-stage host infections of *Amoebophrya*. However, mature stage infections could still be accurately identified in IFCB images and were recorded with much higher sampling frequency.

Another unique strength of the IFCB approach was its ability to reveal cell volume dynamics in addition to simple estimates of species abundance. One of the most striking results from our analysis is the extent to which the *A. fundyense* bloom was segmented into distinct, life cycle stage-associated periods. These periods were marked by concerted shifts in singlet cell volume (transition from vegetative division to gametogenesis) and changes in the amplitude of diel volume oscillations (transition from gametogenesis to zygosis; Fig. 6). In several respects, the observations collected here dramatically alter our conception of *A. fundyense* behavior through its planktonic life cycle stages. These new insights into the behavior of *A. fundyense* are outlined below and are each being explored further through continued deployments of IFCBs in the NMS.

Rapid vegetative division during *A. fundyense* bloom development

Development of the 2012 *A. fundyense* bloom in Salt Pond occurred earlier than in any previous year for which data are available yet water temperatures near the bloom's peak were substantially cooler than is typical (Ralston et al. 2014). The bloom was also among the most intense ever recorded at this site, causing patches of "red water" to be visible in some areas of the pond during the week of 15 April. A puzzling aspect of this observation has been uncertainty about how such an intense bloom arose.

Specific division rates of *A. fundyense* do not typically exceed 0.20 d^{-1} when grown in batch cultures at temperatures < 11°C (Stock et al. 2005 and references therein; Fig. 7 and batch culture data not shown) but the Salt Pond bloom accumulated at an average rate 0.30 d^{-1} from 25 March to 16 April, a period when temperatures increased from 7°C to 11°C near the surface (and were less at depth). Although accumulation encompasses bloom development processes in addition to cell division (e.g., cyst germination or introduction of cells via advection from outside the pond), these have been shown to be insignificant at the study site. Past and ongoing investigations have shown that Salt Pond does not host nearly enough germinable cysts to significantly affect population growth rates during the later stages of development (Anderson et al. 1983; Anderson unpubl.). The Salt Pond bloom is also well isolated from southern NMS blooms, limiting the potential for these other populations to be advected in (Crespo et al. 2011; Ralston et al. 2014). Given the limited potential for inputs from germination and advection, the fact that observed accumulation rates exceed laboratory values suggests that cell loss rates due to grazing, encystment or leakage from the pond are small. Some grazing clearly does occur since some *A. fundyense* cells were observed being ingested by microzooplankton (Fig. 2) and larger mesozooplankton (Petitpas et al. 2015). Therefore the discrepancy between the observed *A. fundyense* accumulation rate and its division rate in culture is perhaps even greater.

Another implication of the high accumulation rates is that culture experiments have substantially underestimated the true growth potential of natural blooms. Because division by *A. fundyense* was strongly phased, IFCB images of *A. fundyense* singlets could be used to estimate minimum values of μ_{div} using a cell volume-based approach that accurately estimated division in the continuous culture (Fig. 7). Generally, these IFCB-based estimates were greater than the overall rate of accumulation in Salt Pond and increased steadily, reaching a maximum > 0.4 d^{-1}, more than twice the rate observed in the continuous culture incubated at comparable temperature and light intensity (Fig. 6). The estimated rates of division are also double those recorded from batch cultures of several other isolates including an additional one from the NMS (Watras et al. 1982; Anderson et al. 1984; Anderson unpubl.).

Importantly, the division rates were calculated through a set of assumptions meant to underestimate rather than overestimate their true values. Very similar μ_{div} estimates from DNA content measurements taken 3 April and 10 April lend support to the cell volume-based estimates although these may also have been low (Table 1). At comparable division rates, the 2c, G2 and M phases of the mitotic cycle have been shown to last 10–15 h in batch cultures (Taroncher-Oldenburg et al. 1999), so 2c cells likely divided sometime between the weekly survey sampling time and the next night's phased division. Still, some cells may have undertaken DNA replication (S phase) after the weekly sampling times and would not have been included in μ_{div} estimates from the DNA measurements.

The assumptions underlying the cell volume-based calculations of μ_{div} were largely supported by data from the IFCB record. The first of these assumptions, that individual cells do not grow larger during the phased division period, is reasonable because volume shifts (and therefore phased divisions) occurred in darkness, limiting the dividing cells' potential for growth. The second, that all divisions were phased, was assessed directly by examining the proportion of dividing cells in night and daytime samples. Dividing cells were rare (frequencies less than 0.5%), during the early stages of development (28 March–11 April), but became more abundant 13–17 April, a period that spanned the transition from the bloom's development to its gametic phase (Fig. 3). Early on 13 April, the frequency of dividing cells was 2.3% then fell to 0% before reaching a peak of 6.8% overnight on 13–14 April. The proportion fell again to 0% later in the afternoon before reaching 3% the next night (14–15 April) when the oscillations in dividing cell frequency stopped and the frequency remained above 1% through 17 April ($\sim$1 d into the gametic phase of bloom termination).

Additional known sources of error, the restriction to singlet cells and reliance on a single sampling depth, likely further biased estimates to be low. Cell chains are formed through division so their constituent cells are smaller on

average than singlets. While volumes at different depths were not compared during the 2012 deployment, a deployment in Salt Pond in 2013 found that during morning hours (when most *A. fundyense* have divided and migrated to shallower depths) cells remaining at 5 m were ~9% larger than shallower, migrated cells (Brosnahan and Anderson unpubl.). If cells in the 2012 bloom behaved similarly, the constraint of a fixed sampling depth likely caused underestimation of μ_{div} by about 20%.

While the μ_{div} estimates provided here are much greater than typical results from cultures, they are still well below the highest rates reported. Smayda (1996) recorded a specific division rate of 1 d^{-1} from an *A. fundyense* isolate grown under sunlight and speculated that similar rapid growth might trigger blooms. Taroncher-Oldenburg et al. (1997) also reported high division rates (>0.6 d^{-1}) after synchronizing *A. fundyense* cultures with an 82 h dark period. The latter experiments were conducted with fluorescent lights and a 14: 10 light: dark cycle similar to the batch culture experiments reported here, but also used a much higher incubation temperature (20°C) and aeration. Neither the Smayda (1996) nor the Taroncher-Oldengurg et al. (1997) study is representative of conventional approaches used to define "normal" growth in response to changes in temperature, but they provide starting points for future work that seeks to better define the growth potential of *A. fundyense* and other dinoflagellate species from cultures. Ultimately, however, it will continue to be challenging to apply culture-based approaches to understand the behavior of natural populations because the physical and biological factors impacting growth are numerous, diverse and difficult to recreate and manipulate in the laboratory.

The results presented here demonstrate that methods for the estimation of specific division rates in situ may provide more accurate (and greater) values. In addition to the cell volume-based approach employed here, in situ division rates can be estimated from dividing cell (or doublet) frequencies (Chisholm 1981; Campbell et al. 2010) or through the application of size-structured, population matrix models (Sosik et al. 2003; Dugenne et al. 2014; Hunter-Cevera et al. 2014). In the case of *A. fundyense*, the former, frequency of dividing cell approach was made difficult because dividing cells were rare and were not well classified by the 11-subclass machine. Doublet cells, another marker of division, were much more accurately classified but appeared to also have highly variable lifespans; doublets were present in all development phase samples and were sometimes observed forming triplet or quadruplet cells. Both the dividing and doublet subclasses were still informative as markers of division in the population. The frequency of doublets oscillated with a diel cycle similar to mean singlet cell volume throughout the bloom's development phase (about 20% of *A. fundyense* images), then declined steadily to 0% by the end of the bloom's gametic phase. Dividing cells similarly declined to 0% after their surge in abundance late in the bloom's development. A recent version of the size-structured, population matrix-model has been applied to the Salt Pond dataset but its full development is planned for a future study. One of the advantages of this approach is its ability to account for periods of simultaneous division and cell growth as is likely to occur during unphased divisions (Sosik et al. 2003). The primary advantages of the mean volume calculation employed here are its simplicity and its conservatism, the latter making its unusually high division estimates especially noteworthy. *A. fundyense* cells were growing at much higher rates than conventional culture-based experiments indicate, pointing to a basic inadequacy in the culture-based approach. The IFCB and other automated platforms for high frequency observation of individual cells provide a means to address this problem.

What triggers the transition from vegetative division to the formation of gametes?

Several past studies in Salt Pond have noted the absence of stressors that might reduce *A. fundyense* growth and drive the population toward sex (Anderson et al. 1983; Crespo et al. 2011; Brosnahan et al. 2014). More recently, Velo-Suárez et al. (2013) showed that a peak in early stage *Amoebophrya* infections immediately preceded the transition of the 2012 bloom to its gametic phase. In that study it was hypothesized that early stage *Amoebophrya* infections may have stimulated the bloom's dramatic sexual transition, similar to life cycle interactions shown in other dinoflagellate-parasitoid systems (Toth et al. 2004; Chambouvet et al. 2011).

In the IFCB time series, the gametic transition was marked by the rapid conversion of the *A. fundyense* population to relatively small singlet cells that were sometimes observed as fusing pairs (Figs. 2, 6). Small cells were therefore considered gametes and hypothesized as a marker of sexual induction in our analysis of the continuous culture experiment. In the culture, however, no small cells or decrease in mean cell volume was observed after inoculation with dinospores, nor were cells observed fusing as sometimes occurs when clonal cultures are nutrient stressed (Destombe and Cembella 1990). Instead, cell division ceased and cell size grew steadily. This latter result conflicts with our own earlier report that infection did not increase cell size in SPE10-03, another clonal isolate from Salt Pond (Brosnahan et al. 2014). It may be that the different results reflect clone- and/or temperature-dependent differences in infection response, or simply that our previous experiment was sampled too early to record a size increase from infection.

While the continuous culture result does not support our previous speculation that stress from *Amoebophrya* induces sex, the lack of response may also be attributed to insensitivity of the ATSPF7-5 clone or the absence of other signals necessary for sexual induction. Persson et al. (2013) have

suggested that gametes produced in culture are the same size as vegetative cells. If true, perhaps gametes were present in the continuous culture but were also obviously different than those present in the Salt Pond bloom. It is also possible that the severity of the culture infection prevented *A. fundyense* cells from transforming into gametes before being infected. The dinospore-to-host ratio in the culture was comparable to the highest ratios observed during the Salt Pond bloom, and the peak in early grade infections was much greater. Approximately 60% of the cultured cells were infected 1 d after dinospore inoculation, but the peak in early infections 15 April was only 4% of *A. fundyense* in Salt Pond (Velo-Suárez et al. 2014). Further, all of the cells remaining in the culture eventually succumbed to *Amoebophrya* infection, but less than 1% of the Salt Pond population did the same.

Other variables that may be tied to the Salt Pond bloom's sexual transition include increasing temperature stratification during the transition to the gametic phase and the bloom's remarkable intensity. In culture, cyst formation by the congeneric *A. minutum* is most robust when cultures are incubated in warm, freshened media (>22°C and salinity <19; Figueroa et al. 2011). This is similar in one respect to Salt Pond since gametogenesis coincided with neap tides and increasing surface temperatures (Fig. 6). However, no comparable freshening of the pond occurred, nor are major decreases in salinity expected within the NMS due to its lack of riverine inputs. With respect to bloom intensity, cell concentrations recorded during the peak of the bloom were quite high but not necessarily unknown for NMS blooms of *A. fundyense*. The similarity of several years of NMS blooms sampled at weekly intervals as a function of degree-days suggests a concentration-dependent threshold triggering bloom termination (Ralston et al. 2014, 2015). A similar, rapid sexual conversion of *A. fundyense* was also documented when cell concentrations exceeded 10^6 L^{-1} in the Gulf of Maine (McGillicuddy et al. 2014).

Rapid gamete cell division and estimation of new cyst production

Past studies in the NMS have concluded that gametogenesis occurs via a rapid series of divisions to produce nondividing gametes, that in turn fuse to produce planozygotes and eventually new resting cysts (Anderson et al. 1983; Anderson and Lindquist 1985). At first glance, the appearance of large numbers of small gamete cells with the onset of the 2012 bloom's termination appears to support this same mechanism. However, mean cell volume continued to oscillate during the gametic phase, producing estimates of specific division rate greater than observed in the preceding development phase ($\sim$0.5 d^{-1}). This is even more surprising given the onset of termination. Observations of grazing did not indicate negative population growth on 17 April, one full day into the bloom's decline (Petitpas et al. 2015), suggesting that the volume oscillations might reflect cycles of gamete fusion and diploid division. Similar behavior has been described in both *A. minutum* and *A. tamutum* (Figueroa et al. 2006; Figueroa unpubl.). If such zygotic divisions were occurring, perhaps the shift in dynamics explains the disagreement between DNA- and cell volume-based estimates of μ_{div} from 17 April (Table 1). It also is noteworthy that the gametic divisions continued to be phased in a similar pattern to divisions by development phase cells, but no similar rhythmicity was apparent in the frequency of fusing gametes.

The onset of termination in spite of high division rates might also suggest that gamete cells are especially vulnerable to grazing or leakage from the pond during ebbs. Concerted gametogenesis may maximize the likelihood of gamete fusion and also overwhelm the capacity of the grazer community to consume gamete cells.

Whether divisions during the gametic phase were by haploid or diploid cells, their occurrence complicates estimation of zygote production from observations of fusing gametes. Sums of fusing gamete frequencies cannot simply be converted to new zygote production if the gamete population itself is growing or if new zygotes can reverse their progression through their life cycle. Instead, because the transition to the zygote phase was also concerted, a first order approximation of new cyst production can be made from the initial cell concentration at the start of the zygotic period. From the rate of decline observed through the gametic phase and the vertical distribution of cell abundance observed 17 April, the average concentration of new planozygotes at the beginning of the zygotic phase was likely about 50,000 L^{-1}. Assuming all of these transformed to new cysts, average deposition on the pond's bottom would be approximately 15,000 cysts cm^2, comparable to the cyst deposition observed after the Salt Pond bloom in 2013, a year when peak cell concentrations again were $>10^6$ cells L^{-1} (Brosnahan, Fischer, and Anderson unpubl.). Because the bloom's rate of decline during its zygotic phase (-1.0 d^{-1}) far exceeded estimates of overall losses due to grazing and parasitism (approximately -0.3 d^{-1}; Petitpas et al. 2015), encystment was likely the dominant factor leading to bloom termination. We are unable to confirm this conclusion, however, because no comparable time series of cyst abundance during the 2012 bloom exists. We have addressed this shortfall in subsequent NMS deployments of the IFCB system and will further explore the conversion of planktonic blooms to new cysts in future studies.

Deployments of the IFCB like the one described here maximize this instrument's potential to characterize the immediate causes of *A. fundyense* bloom development and decline. At Salt Pond we are able to resolve critical transitions in the population dynamics of this species including the timing of gamete formation and cell fusion and also show the critical importance of these life cycle processes to bloom

termination. Likewise high frequency IFCB observations combined with the retentive characteristics of the Salt Pond site have revealed population division rates that are much greater than previously predicted from culture studies. In many respects these observations are radically altering our conception of behavior during *A. fundyense*'s planktonic life cycle stages. With the IFCB and its accompanying support raft we can observe and ultimately understand many aspects of dinoflagellate life history that until now were either elusive or intractable.

References

Anderson, D. M., S. W. Chisholm, and C. J. Watras. 1983. Importance of life cycle events in the population dynamics of *Gonyaulax tamarensis*. Mar. Biol. **76**: 179–189. doi:10.1007/BF00392734

Anderson, D., D. Kulis, and B. Binder. 1984. Sexuality and cyst formation in the dinoflagellate *Gonyaulax tamarensis*: Cyst yield in batch cultures. J. Phycol. **20**: 418–425. doi:10.1111/j.0022-3646.1984.00418.x

Anderson, D., and N. Lindquist. 1985. Time-course measurements of phosphorus depletion and cyst formation in the dinoflagellate *Gonyaulax tamarensis* Lebour. J. Exp. Mar. Biol. Ecol. **86**: 1–13. doi:10.1016/0022-0981(85)90039-5

Anderson, D., and K. Stolzenbach. 1985. Selective retention of two dinoflagellates in a well-mixed estuarine embayment: The importance of diel vertical migration and surface avoidance. Mar. Ecol. Prog. Ser. **25**: 39–50. doi:10.3354/meps025039

Anderson, D. M., D. M. Kulis, B. A. Keafer, K. E. Gribble, R. Marin, and C. A. Scholin. 2005. Identification and enumeration of *Alexandrium* spp. from the Gulf of Maine using molecular probes. Deep-Sea Res. II **52**: 2467–2490. doi:10.1016/j.dsr2.2005.06.015

Anderson, D. M., T. J. Alpermann, A. D. Cembella, Y. Collos, E. Masseret, and M. Montresor. 2012. The globally distributed genus *Alexandrium*: Multifaceted roles in marine ecosystems and impacts on human health. Harmful Algae **14**: 10–35. doi:10.1016/j.hal.2011.10.012

Boedigheimer, M. J., and J. Ferbas. 2008. Mixture modeling approach to flow cytometry data. Cytometry A **73**: 421–429. doi:10.1002/cyto.a.20553

Breiman, L. 2001. Random forests. Mach. Learn. **45**: 5–32. doi:10.1023/A:1010933404324

Brosnahan, M. L., S. Farzan, B. A. Keafer, H. M. Sosik, R. J. Olson, and D. M. Anderson. 2014. Complexities of bloom dynamics in the toxic dinoflagellate *Alexandrium fundyense* revealed through DNA measurements by imaging flow cytometry coupled with species-specific rRNA probes. Deep-Sea Res. II. **103**: 185–198. doi:10.1016/j.dsr2.2013.05.034

Cachon, J. 1969. Contribution à l'étude des péridiniens parasites: Cytologie, cycles évolutifs. Ann. Sci. Nat. Zool. **6**: 1–158.

Campbell, L., R. J. Olson, H. M. Sosik, A. Abraham, D. W. Henrichs, C. J. Hyatt, and E. J. Buskey. 2010. First harmful *Dinophysis* (Dinophyceae, Dinophysiales) bloom in the U.S. is revealed by automated imaging flow cytometry. J. Phycol. **46**: 66–75. doi:10.1111/j.1529-8817.2009.00791.x

Chambouvet, A., P. Morin, D. Marie, and L. Guillou. 2008. Control of toxic marine dinoflagellate blooms by serial parasitic killers. Science **322**: 1254–1257. doi:10.1126/science.1164387

Chambouvet, A., C. Alves-de-Souza, V. Cueff, D. Marie, S. Karpov, and L. Guillou. 2011. Interplay between the parasite *Amoebophyra* sp. (Alveolata) and the cyst formation of the red tide dinoflagellate *Scrippsiella trochoidea*. Protist **162**: 637–649. doi:10.1016/j.protis.2010.12.001

Chisholm, S. W. 1981. Temporal patterns of cell division in unicellular algae. Can. Bull. Fish. Aquat. Sci. **210**: 150–181.

Crespo, B. G., B. A. Keafer, D. K. Ralston, H. Lind, D. Farber, and D. M. Anderson. 2011. Dynamics of *Alexandrium fundyense* blooms and shellfish toxicity in the Nauset Marsh System of Cape Cod (Massachusetts, USA). Harmful Algae **12**: 26–38. doi:10.1016/j.hal.2011.08.009

Crusius, J., and others. 2005. Submarine groundwater discharge to a small estuary estimated from radon and salinity measurements and a box model. Biogeosciences **2**: 141–157. doi:10.5194/bg-2-141-2005

Destombe, C., and A. Cembella. 1990. Mating-type determination, gametic recognition and reproductive success in *Alexandrium excavatum* (Gonyaulacales, Dinophyta), a toxic red-tide dinoflagellate. Phycologia **29**: 316–325. doi:10.2216/i0031-8884-29-3-316.1

Dugenne, M., M. Thyssen, D. Nerini, C. Mante, J.-C. Poggiale, N. Garcia, and G. J. Grégori. 2014. Consequence of a sudden wind event on the dynamics of a coastal phytoplankton community: An insight into specific population growth rates using a single cell high frequency approach. Front. Microbiol. **5**: 1–14. doi:10.3389/fmicb.2014.00485

DuRand, M. D., and R. J. Olson. 1998. Diel patterns in optical properties of the chlorophyte *Nannochloris* sp.: Relating individual-cell to bulk measurements. Limnol. Oceanogr. **43**: 1107–1118. doi:10.4319/lo.1998.43.6.1107

Figueroa, R. I., I. Bravo, and E. Garcés. 2006. Multiple routes of sexuality in *Alexandrium taylori* (Dinophyceae) in culture. J. Phycol. **42**: 1028–1039. doi:10.1111/j.1529-8817.2006.00262.x

Figueroa, R. I., J. A. Vázquez, A. Massanet, M. A. Murado, and I. Bravo. 2011. Interactive effects of salinity and temperature on planozygote and cyst formation of *Alexandrium minutum* (Dinophyceae) in culture. J. Phycol. **47**: 13–24. doi:10.1111/j.1529-8817.2010.00937.x

Fritz, L., and M. Nass. 1992. Development of the endoparasitic dinoflagellate *Amoebophrya ceratii* within host dinoflagellate species. J. Phycol. **28**: 312–320. doi:10.1111/j.0022-3646.1992.00312.x

Hallegraeff, G. M. 2010. Ocean climate change, phytoplankton community responses, and harmful algal blooms: A formidable predictive challenge. J. Phycol. **46**: 220–235. doi:10.1111/j.1529-8817.2010.00815.x

Hunter-Cevera, K. R., M. G. Neubert, A. R. Solow, R. J. Olson, A. Shalapyonok, and H. M. Sosik. 2014. Diel size distributions reveal seasonal growth dynamics of a coastal phytoplankter. Proc. Natl. Acad. Sci. **111**: 9852–9857. doi:10.1073/pnas.1321421111

John, U., R. W. Litaker, M. Montresor, S. Murray, M. L. Brosnahan, and D. M. Anderson. 2014. Formal revision of the *Alexandrium tamarense* species complex (Dinophyceae): The introduction of five species with emphasis on molecular-based (rDNA) classification. Protist **165**: 779–804. doi:10.1016/j.protis.2014.10.001

Li, Y., R. He, D. J. McGillicuddy, Jr., D. M. Anderson, and B. A. Keafer. 2009. Investigation of the 2006 *Alexandrium fundyense* bloom in the Gulf of Maine: In-situ observations and numerical modeling. Cont. Shelf Res. **29**: 2069–2082. doi:10.1016/j.csr.2009.07.012

McGillicuddy, D. J., and others. 2014. A red tide of *Alexandrium fundyense* in the Gulf of Maine. Deep-Sea Res. II. **103**: 174–184. doi:10.1016/j.dsr2.2013.05.011

Miyazono, A., S. Nagai, I. Kudo, and K. Tanizawa. 2012. Viability of *Alexandrium tamarense* cysts in the sediment of Funka Bay, Hokkaido, Japan: Over a hundred year survival times for cysts. Harmful Algae **16**: 81–88. doi:10.1016/j.hal.2012.02.001

Moberg, E. A., and H. M. Sosik. 2012. Distance maps to estimate cell volume from two-dimensional plankton images. Limnol. Oceanogr.: Methods **10**: 278–288. doi:10.4319/lom.2012.10.278

Olson, R. J., and S. W. Chisholm. 1986. Effects of light and nitrogen limitation on the cell cycle of the dinoflagellate *Amphidinium carteri*. J. Plankton Res. **8**: 785–793. doi:10.1093/plankt/8.4.785

Olson, R., and H. M. Sosik. 2007. A submersible imaging-in-flow instrument to analyze nano-and microplankton: Imaging FlowCytobot. Limnol. Oceanogr. Methods **5**: 195–203. doi:10.4319/lom.2007.5.195

Peacock, E. E., R. J. Olson, and H. M. Sosik. 2014. Parasitic infection of the diatom *Guinardia delicatula*, a recurrent and ecologically important phenomenon on the New England Shelf. Mar. Ecol. Prog. Ser. **503**: 1–10. doi:10.3354/meps10784

Persson, A., B. C. Smith, G. H. Wikfors, and J. H. Alix. 2013. Differences in swimming pattern between life cycle stages of the toxic dinoflagellate *Alexandrium fundyense*. Harmful Algae **21**: 36–43. doi:10.1016/j.hal.2012.11.005

Petitpas, C. M., J. T. Turner, B. A. Keafer, D. J. McGillicuddy, Jr., and D. M. Anderson. 2015. Zooplankton community grazing impact on a toxic bloom of *Alexandrium fundyense* in the Nauset Marsh system, Cape Cod, Massachusetts, USA. Harmful Algae **47**: 42–55. doi:10.1016/j.hal.2015.05.010

Pfiester, L. A., and D. M. Anderson. 1987. Dinoflagellate reproduction, p. 611–648. *In* F. J. R. Taylor [ed.], The biology of the dinoflagellates. Botanical Monographs.

Ralston, D. K., B. A. Keafer, M. L. Brosnahan, and D. M. Anderson. 2014. Temperature dependence of an estuarine harmful algal bloom: Resolving interannual variability in bloom dynamics using a degree-day approach. Limnol. Oceanogr. **59**: 1112–1126. doi:10.4319/lo.2014.59.4.1112

Ralston, D. K., M. L. Brosnahan, S. E. Fox, and D. M. Anderson. 2015. Temperature and residence time controls on an estuarine harmful algal bloom: Modeling hydrodynamics and *Alexandrium fundyense* in Nauset estuary. Estuaries Coast. doi:10.1007/s12237-015-9949-z

Smayda, T. J. 1996. Dinoflagellate bloom cycles: What is the role of cellular growth rate and bacteria? p. 331–334. In T. Yasumoto, Y. Oshima, and Y. Fukuyo [eds.], Harmful and toxic algal blooms. UNESCO.

Sosik, H. M., R. J. Olson, M. G. Neubert, A. Shalapyonok, and A. R. Solow. 2003. Growth rates of coastal phytoplankton from time-series measurements with a submersible flow cytometer. Limnol. Oceanogr. **48**: 1756–1765. doi: 10.4319/lo.2003.48.5.1756

Sosik, H. M., and R. J. Olson. 2007. Automated taxonomic classification of phytoplankton sampled with imaging inflow cytometry. Limnol. Oceanogr.: Methods **5**: 204–216. doi:10.4319/lom.2007.5.204

Stock, C. A., D. J. McGillicuddy, Jr., A. R. Solow, and D. M. Anderson. 2005. Evaluating hypotheses for the initiation and development of *Alexandrium fundyense* blooms in the western Gulf of Maine using a coupled physical–biological model. Deep-Sea Res. II. **52**: 2715–2744. doi:10.1016/j.dsr2.2005.06.022

Taroncher-Oldenburg, G., D. Kulis, and D. Anderson. 1997. Toxin variability during the cell cycle of the dinoflagellate *Alexandrium fundyense*. Limnol. Oceanogr. **42**: 1178–1188. doi:10.4319/lo.1997.42.5_part_2.1178

Taroncher-Oldenburg, G., D. M. Kulis, and D. M. Anderson. 1999. Coupling of saxitoxin biosynthesis to the G1 phase of the cell cycle in the dinoflagellate *Alexandrium fundyense*: Temperature and nutrient effects. Nat. Toxins **7**: 207–219.

Toth, G. B., F. Noren, E. Selander, and H. Pavia. 2004. Marine dinoflagellates show induced life-history shifts to escape parasite infection in response to water-borne signals. Proc. R. Soc. Lond. B. Biol. **271**: 733–738. doi:10.1098/rspb.2003.2654

Velo-Suárez, L., M. L. Brosnahan, D. M. Anderson, and D. J. McGillicuddy, Jr. 2013. A quantitative assessment of the role of the parasite *Amoebophrya* in the termination of *Alexandrium fundyense* blooms within a small coastal embayment. PLoS One **8**: e81150. doi:10.1371/journal.pone.0081150.g008

Watras, C. J., S. W. Chisholm, and D. M. Anderson. 1982. Regulation of growth in an estuarine clone of Gonyaulax

tamarensis Lebour: Salinity-dependent temperature responses. J. Exp. Mar. Biol. Ecol. **62**: 25–37. doi:10.1016/0022-0981(82)90214-3

Acknowledgments

Special thanks to Bruce Keafer, Kerry Norton, David Kulis, Yan Gao and other staff and student members of D. Anderson's laboratory for assistance in sample collection and preparation of cultures, to Micheil Boesel for technical assistance during the design and construction of the IFCB support raft, to Krista Lee and staff at the Cape Cod National Seashore Salt Pond Visitor Center for assistance in setting up the raft communication system, and to Linda Amaral-Zettler, Leslie Murphy, and Julie Reveillaud who assisted with *Amoebphrya* surveys at Salt Pond. This work was supported by the National Science Foundation (OCE-0430724, OCE-0911031, and OCE-1314642) and National Institutes of Health (NIEHS-1P50-ES021923-01) through the Woods Hole Center for Oceans and Human Health, by National Park Service (NPS) Cooperative Agreement H238015504, by the Gordon and Betty Moore Foundation (Grant #2649 to HMS), and by an award from the Access to the Sea program at the Woods Hole Oceanographic Institution. Additional support was provided through a Marie Curie International Outgoing Fellowship to L. Velo-Suárez (IOF; grant agreement: MOHAB PIOF-GA-252260).

Submitted 29 January 2015
Revised 19 June 2015
Accepted 20 July 2015

Associate editor: Susanne Menden-Deuer